International Journal of Computer Information Systems and Industrial Management Applications
ISSN 2150-7988 Volume 18(2s) 2026 pp. 217-242
https://doi.org/10.70917/ijcisim-2026-2075
Article

HYBRID QUANTUM-CLASSICAL ARCHITECTURES FOR OPTIMIZING MACHINE LEARNING TRAINING SPEED AND ACCURACY IN BRAIN TUMOR DETECTION

Prakash Mishra[1], Rakesh Kumar[2]

[1] Rabindranath Tagore University, Bhopal, India. Mishra.prakash32@gmail.com
[2] Rabindranath Tagore University, Bhopal, India. rakeshmittan@gmail.com
Corresponding Author: Prakash Mishra (Mishra.prakash32@gmail.com)

Abstract: Brain tumor classification remains a challenging task due to the complex heterogeneity of glioma characteristics and the limitations of conventional machine learning approaches in effectively integrating multimodal biomedical data. Recent advances in quantum machine learning have demonstrated promising capabilities for handling high-dimensional data; however, existing models often suffer from limited feature representation, insufficient multimodal integration, and optimization challenges. This paper proposes an Enhanced Hybrid Quantum–Classical Architecture (EHQCA) for glioma classification by combining MRI imaging features and TCGA molecular biomarkers within a unified learning framework. The proposed methodology employs ResNet-50 for imaging feature extraction, ensemble feature selection for molecular biomarkers, attention-based multimodal fusion, adaptive amplitude encoding, and a Multi-Layer Variational Quantum Classifier (ML-VQC). A hybrid Adam-SPSA optimization strategy is introduced to improve convergence speed and training stability. Experimental analysis demonstrates that the proposed EHQCA framework achieves superior classification performance, attaining 91.2% accuracy while reducing training epochs compared with existing quantum and classical models. The results highlight the effectiveness of multimodal fusion and quantum-enhanced learning for improving brain tumor diagnosis and supporting precision medicine applications

Keywords: Brain Tumor Classification; Quantum Machine Learning; Hybrid Quantum-Classical Architecture; MRI Imaging; Multimodal Fusion; Variational Quantum Classifier....

1. INTRODUCTION

Brain tumors are among the most critical neurological disorders and represent a significant cause of morbidity and mortality worldwide. Accurate differentiation between Low-Grade Glioma (LGG) and High-Grade Glioma (HGG) is essential for treatment planning, prognosis assessment, and personalized clinical decision-making. Magnetic Resonance Imaging (MRI) remains the primary imaging modality for brain tumor diagnosis because it provides detailed anatomical and pathological information regarding tumor morphology, edema, necrosis, and tissue heterogeneity [25], [28]. In addition to imaging information, molecular biomarkers such as IDH1, EGFR, PTEN, and ATRX have become increasingly important for glioma characterization and World Health Organization (WHO)-based tumor grading [10], [22].

Recent advances in machine learning and deep learning have significantly improved brain tumor classification performance through automated feature extraction and pattern recognition [2], [6], [17]. Convolutional Neural Networks (CNNs), transfer learning models, and ensemble learning approaches have demonstrated promising

diagnostic capabilities using MRI data [4], [6], [14]. Nevertheless, most existing methods rely primarily on a single modality and often fail to exploit complementary information available from molecular biomarkers. Consequently, classification performance may be affected by limited feature diversity and insufficient representation of tumor heterogeneity.

Quantum Machine Learning (QML) has emerged as a promising paradigm that combines quantum computing principles with machine learning techniques to enhance feature representation and computational efficiency [8], [21], [23]. Variational Quantum Classifiers (VQCs), Quantum Neural Networks (QNNs), and hybrid quantum-classical architectures have shown encouraging results in medical image analysis and disease prediction [5], [11], [18]. Despite these developments, current QML-based brain tumor classification models often suffer from limitations such as restricted feature encoding capacity, shallow circuit architectures, optimization instability, and poor integration of multimodal biomedical data [7], [19], [22].

To address these challenges, this study proposes an Enhanced Hybrid Quantum–Classical Architecture (EHQCA) that integrates MRI imaging features and TCGA molecular biomarkers within a unified multimodal framework. The proposed architecture combines ResNet-50-based feature extraction, ensemble molecular feature selection, attention-based multimodal fusion, adaptive amplitude quantum encoding, a Multi-Layer Variational Quantum Classifier (ML-VQC), and a hybrid Adam-SPSA optimization strategy. By leveraging both imaging phenotypes and molecular genotypes, the proposed framework aims to improve classification accuracy, reduce training complexity, and enhance compatibility with Noisy Intermediate-Scale Quantum (NISQ) devices.

The major contributions of this work are summarized as follows:

Development of a multimodal EHQCA framework integrating MRI imaging and TCGA molecular biomarkers.

Introduction of an attention-based fusion mechanism for learning cross-modal relationships.

Proposal of adaptive amplitude encoding for efficient compression of 32-dimensional features into a 5-qubit quantum state.

Design of a Multi-Layer Variational Quantum Classifier with adaptive circuit depth for improved expressibility.

Implementation of a hybrid Adam-SPSA optimization strategy for faster convergence and enhanced training stability.

Comprehensive evaluation through ablation studies, circuit-depth analysis, encoding strategy comparison, and cross-validation experiments.

The remainder of this paper is organized as follows. Section 2 reviews recent literature on brain tumor classification, multimodal learning, and quantum machine learning. Section 3 presents the proposed EHQCA methodology. Section 4 describes implementation details, datasets, and experimental settings. Section 5 discusses the obtained results and comparative analyses. Finally, Section 6 concludes the paper and outlines future research directions.

2. LITERATURE REVIEW

Brain tumor classification has attracted significant attention due to its importance in early diagnosis and treatment planning. Traditional machine learning approaches have utilized handcrafted imaging features combined with classifiers such as Support Vector Machines (SVMs), Random Forests, and ensemble methods to distinguish tumor categories [28]. Although these methods demonstrated moderate performance, their reliance on manual feature engineering limited their ability to capture complex tumor characteristics.

The emergence of deep learning significantly improved medical image analysis by enabling automatic extraction of hierarchical imaging features. Berghout [25] reviewed the growing impact of deep learning techniques in brain tumor detection and highlighted the effectiveness of CNN-based architectures for MRI analysis. Amin et al. [6] proposed an ensemble transfer learning framework integrated with a Variational Quantum Classifier and reported improved classification performance compared with conventional approaches. Similarly, Muniasamy et al. [2] investigated hybrid quantum-assisted deep learning models for MRI-based brain tumor classification, demonstrating the potential of integrating classical and quantum learning paradigms.

Recent studies have increasingly explored quantum computing technologies in healthcare applications. Rahimi and Asadi [10] reviewed oncological applications of quantum machine learning and emphasized its capability to

process complex biomedical datasets. Orka et al. [8] presented a systematic review of quantum deep learning in neuroinformatics, identifying medical imaging as one of the most promising application domains. Mohammadisavadkoohi et al. [23] further summarized recent advances in quantum machine learning classification methods and highlighted challenges related to scalability, noise sensitivity, and optimization.

Several researchers have investigated quantum-enhanced brain tumor classification models. Ahmed et al. [5] introduced Quantumedics, a hybrid CNN–quantum framework for brain tumor diagnosis. Cui and Huang [11] demonstrated that stronger quantum entanglement improves classification capability in quantum neural networks for brain tumor detection. Ramos-Villena et al. [18] proposed a hybrid quantum model for tumor classification, while Akpinar et al. [22] developed a quantum-enhanced classifier using DNA microarray gene expression profiles. Although these studies demonstrated the feasibility of quantum learning in neuro-oncology, most relied on a single data modality and relatively shallow quantum architectures.

Hybrid quantum-classical learning has emerged as a practical solution for current NISQ devices. Phalak and Ghosh [1] proposed shot optimization techniques to accelerate training in quantum machine learning architectures. Gencer and Gencer [4] introduced a hybrid deep learning framework incorporating quantum genetic optimization for brain tumor classification. Ait Haddou and Bennai [19] developed an explainable hybrid quantum-classical model for tumor diagnosis, highlighting the importance of interpretability in clinical applications. Similarly, Little Lion Scientific [20] proposed a quantum-inspired CNN architecture with explainability analysis for medical imaging tasks.

Feature encoding represents another critical challenge in quantum machine learning. CompressedMedIQ proposed by Chen et al. [24] demonstrated efficient processing of high-dimensional neuroimaging data using compressed quantum representations. Balasubramani et al. [29] investigated quantum-enhanced neural networks for medical image compression, showing the effectiveness of compact quantum feature representations. However, conventional angle encoding and feature map approaches often require a large number of quantum gates and may become inefficient for high-dimensional biomedical data.

Optimization strategies also play an important role in quantum model performance. Suneel et al. [26] and Shahriyar and Tanbhir [27] reported that optimization instability remains one of the primary limitations of current quantum machine learning frameworks. SPSA-based optimization has demonstrated robustness in noisy quantum environments, whereas gradient-based methods offer faster initial convergence [21], [23]. Consequently, hybrid optimization approaches have gained increasing attention for balancing convergence speed and optimization stability.

Despite significant progress, several research gaps remain. First, many existing studies rely solely on MRI images or molecular biomarkers and do not exploit complementary multimodal information [2], [6], [22]. Second, current quantum models frequently employ shallow circuits with limited representational capability [11], [18]. Third, efficient quantum encoding and optimization strategies for high-dimensional biomedical datasets remain insufficiently explored [24], [27]. Finally, the integration of attention-based multimodal fusion with adaptive quantum architectures has received limited investigation [34][35].

To address these limitations, the proposed EHQCA framework integrates MRI imaging features and TCGA molecular biomarkers through an attention-based multimodal fusion mechanism and processes the resulting representation using adaptive amplitude encoding and a Multi-Layer Variational Quantum Classifier. By combining advanced classical feature learning with quantum-enhanced classification, the proposed framework seeks to improve classification accuracy, convergence efficiency, scalability, and clinical applicability for glioma diagnosis.

3. PROPOSED METHODOLOGY

The proposed methodology follows the **Enhanced Hybrid Quantum–Classical Architecture (EHQCA)** shown in the figure 1(a). The system integrates **MRI imaging data** and **TCGA molecular biomarkers** for binary classification of brain tumors into **LGG** and **HGG**. The methodology is organized into eight major stages: data acquisition, preprocessing, CNN feature extraction, molecular feature selection, multimodal fusion, adaptive amplitude encoding, multi-layer VQC classification, and hybrid optimization. This architecture is aligned with the uploaded document's EHQCA pipeline, which combines ResNet-50 MRI features, selected TCGA biomarkers, 32-dimensional fusion, 5-qubit amplitude encoding, and ML-VQC classification.

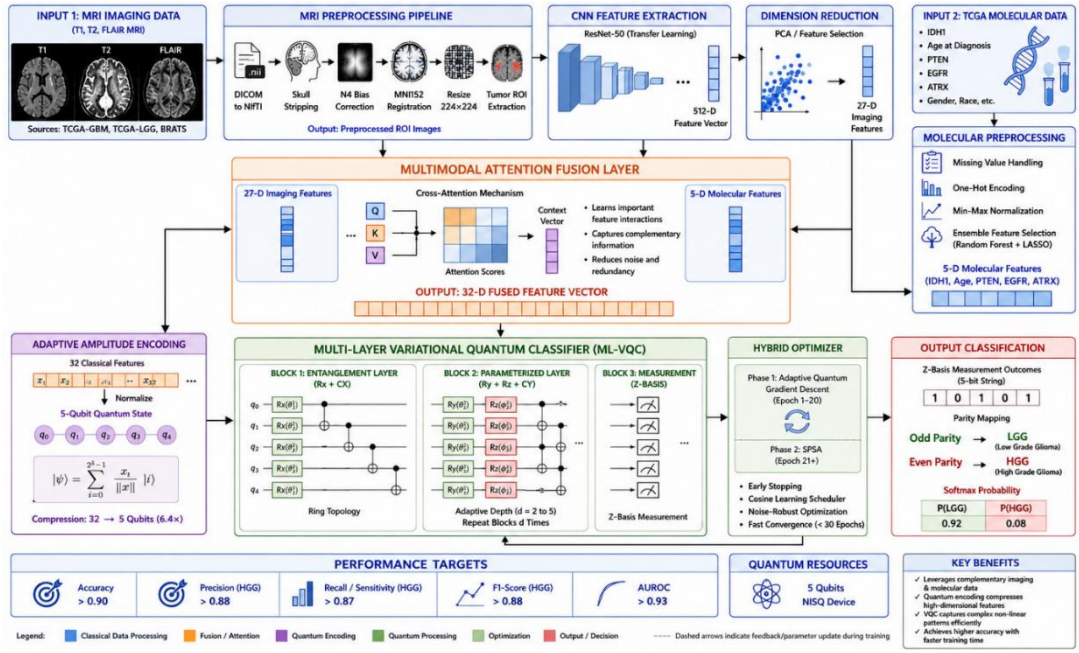

Figure 1(a). Enhanced Hybrid Quantum–Classical Architecture (EHQCA)

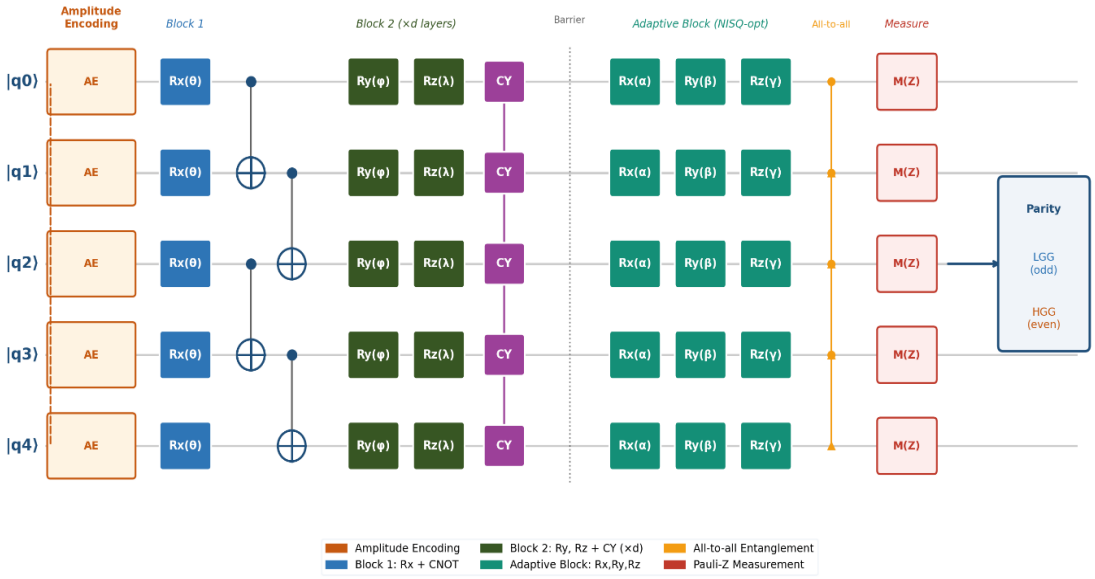

Figure 1(b). Qubit Multi-Layer Variational Quantum Circuit (ML-VQC) Architecture of the Proposed EHQCA Framework

Figure 1(b) illustrates the architecture of the proposed **5-Qubit Multi-Layer Variational Quantum Classifier (ML-VQC)** employed within the EHQCA framework for glioma classification. The circuit is designed to efficiently process the 32-dimensional multimodal feature vector generated after attention-based fusion of MRI imaging and molecular biomarker features. The architecture consists of four major stages: adaptive amplitude encoding, multi-layer quantum feature transformation, adaptive quantum processing, and measurement-based classification.

The first stage performs **adaptive amplitude encoding (AE)**, where the normalized 32-dimensional fused feature vector is mapped into the amplitudes of a five-qubit quantum state. This encoding strategy enables efficient compression of high-dimensional classical information into a low-dimensional quantum representation while

minimizing the number of required qubits. Each qubit is initialized in the quantum ground state and subsequently prepared according to the encoded amplitudes.

Following feature encoding, **Block 1** applies parameterized rotation gates $R_x(\theta)$on each qubit, followed by a ring-topology CNOT entanglement structure. This layer introduces initial quantum correlations among neighboring qubits and enables the circuit to capture dependencies between multimodal features. The entanglement operation allows information encoded within individual qubits to be distributed throughout the quantum system, thereby increasing representational capacity.

The second stage, **Block 2**, consists of repeated parameterized layers containing $R_y(\phi)$, $R_z(\lambda)$, and controlled-Y (CY) gates. These layers form the core variational component of the classifier and are repeated according to the selected circuit depth. The parameterized rotations learn nonlinear feature transformations, while CY gates strengthen entanglement and enhance the expressibility of the quantum model. By stacking multiple layers, the ML-VQC can model increasingly complex decision boundaries required for distinguishing low-grade glioma (LGG) from high-grade glioma (HGG).

After the variational layers, an **adaptive NISQ-optimized quantum block** is introduced. This stage contains additional trainable $R_x(\alpha)$, $R_y(\beta)$, and $R_z(\gamma)$gates that dynamically adjust the circuit representation according to the complexity of the input data. The adaptive block improves robustness against quantum noise and helps maintain classification performance on current Noisy Intermediate-Scale Quantum (NISQ) hardware.

An **all-to-all entanglement layer** is subsequently applied to strengthen global interactions among qubits. Unlike local entanglement structures, this layer enables information sharing across the entire quantum register and facilitates learning of long-range dependencies between imaging and molecular features. Such global correlations are particularly important for multimodal biomedical datasets where clinically relevant relationships may exist across different feature groups.

In the final stage, **Pauli-Z measurements** are performed on all five qubits. The resulting measurement outcomes form a five-bit binary string that is processed using a parity mapping mechanism. According to the proposed classification strategy, odd parity states are associated with the LGG class, whereas even parity states correspond to the HGG class. The measured outputs are subsequently converted into probabilistic class scores using a softmax function, generating the final prediction.

3.1 Data Acquisition

The proposed framework uses two input modalities:

Input 1: MRI Imaging Data

MRI scans are collected from T1-weighted, T2-weighted, and FLAIR sequences. These sequences provide complementary structural and pathological information about tumor region, edema, necrosis, and contrast enhancement.

Let the MRI input for the i^{th}patient be represented as:

$$X_i^{MRI} = \{X_i^{T1}, X_i^{T2}, X_i^{FLAIR}\} \ (1)$$

where X_i^{T1}, X_i^{T2}, and X_i^{FLAIR}represent the three MRI modalities for the same patient.

Input 2: TCGA Molecular Data

The molecular dataset includes clinical and genomic biomarkers such as **IDH1, age at diagnosis, PTEN, EGFR, ATRX**, and other molecular features.

The molecular input vector is represented as:

$$X_i^{MOL} = \{x_{i1}, x_{i2}, x_{i3}, \dots, x_{im}\} \ (2)$$

where $m$denotes the total number of molecular and clinical attributes.

3.2 MRI Preprocessing Pipeline

MRI images are first standardized to reduce acquisition noise and anatomical variability. The preprocessing steps include DICOM-to-NIfTI conversion, skull stripping, N4 bias correction, MNI152 registration, resizing, and tumor ROI extraction.

The MRI preprocessing operation is defined as:

$$\hat{X}_i^{MRI} = P_{MRI}(X_i^{MRI}) \quad (3)$$

where $P_{MRI}(\cdot)$represents the complete MRI preprocessing function and $\hat{X}_i^{MRI}$is the preprocessed MRI image.

Each MRI slice is resized to a fixed spatial dimension:

$$\hat{X}_i^{MRI} \in R^{224\times224\times c} \quad (4)$$

where $c$denotes the number of MRI channels or sequences.

3.3 CNN-Based MRI Feature Extraction

After preprocessing, the MRI images are passed through a **ResNet-50** convolutional neural network. The final classification layer of ResNet-50 is removed, and the network is used as a feature extractor.

The CNN feature extraction process is expressed as:

$$F_i^{MRI} = f_{CNN}(\hat{X}_i^{MRI}; \theta_{CNN}) \quad (5)$$

where:

$f_{CNN}$is the ResNet-50 feature extractor,

θ_{CNN}represents CNN parameters,

$F_i^{MRI}$is the extracted imaging feature vector.

The output feature vector is:

$$F_i^{MRI} \in R^{512} \quad (6)$$

To reduce dimensionality, PCA or feature selection is applied:

$$Z_i^{MRI} = PCA(F_i^{MRI}) \quad (7)$$

where:

$$Z_i^{MRI} \in R^{27} \quad (8)$$

Thus, the 512-dimensional CNN feature vector is reduced to **27 important imaging features**.

3.4 Molecular Data Preprocessing and Feature Selection

The molecular data undergoes missing value handling, one-hot encoding, and min-max normalization.

Min-max normalization is performed as:

$$x'_{ij} = \frac{x_{ij} - x_j^{min}}{x_j^{max} - x_j^{min}} \quad (9)$$

where:

$x_{ij}$is the original value of feature $j$for patient i,

$x_j^{min}$and $x_j^{max}$are the minimum and maximum values of feature j,

$x'_{ij}$is the normalized value.

After preprocessing, ensemble feature selection is applied using methods such as Random Forest, LASSO, and statistical ranking.

The selected molecular feature vector is:

$$Z_i^{MOL} = FS(X_i^{MOL}) \quad (10)$$

where:

$$Z_i^{MOL} = \{IDH1, Age, PTEN, EGFR, ATRX\} \quad (11)$$

and:

$$Z_i^{MOL} \in R^5 \quad (12)$$

3.5 Multimodal Attention Fusion Layer

The 27-dimensional MRI feature vector and 5-dimensional molecular feature vector are combined to form a 32-dimensional fused representation.

The concatenated feature vector is first defined as:

$$Z_i = [Z_i^{MRI}; Z_i^{MOL}] \quad (13)$$

where:

$$Z_i \in R^{32} \quad (14)$$

To learn cross-modal relationships, an attention-based fusion mechanism is applied.

The query, key, and value matrices are computed as:

$$Q = Z_i^{MOL} W_Q \quad (15) \quad K = Z_i^{MRI} W_K \quad (16) \quad V = Z_i^{MRI} W_V \quad (17)$$

where W_Q, W_K, and W_V are trainable weight matrices.

The attention score is calculated as:

$$A_i = Softmax\left(\frac{QK^T}{\sqrt{d_k}}\right) \quad (18)$$

where d_k is the key dimension used for scaling.

The fused multimodal representation is obtained as:

$$F_i^{Fusion} = A_i V + \alpha Z_i^{MOL} \quad (19)$$

where α is a learnable scalar that controls the contribution of molecular features.

The final fused vector is:

$$F_i^{Fusion} \in R^{32} \quad (20)$$

This fusion layer helps the model learn complementary relationships between imaging patterns and molecular biomarkers.

3.6 Adaptive Amplitude Quantum Encoding

The 32-dimensional fused vector is encoded into a 5-qubit quantum state using amplitude encoding.

For a normalized input vector F_i^{Fusion}, the quantum state is represented as:

$$|\psi_i\rangle = \sum_{j=0}^{2^n-1} \frac{x_j}{\| x \|} |j\rangle \quad (21)$$

where:

$x_j$is the j^{th}fused feature,

$\| x \|$is the normalization factor,

$n$is the number of qubits.

Since the fused vector has 32 features:

$$2^n = 32 \quad (22)$$

Therefore:

$$n = 5 \quad (23)$$

Thus, 32 classical features are compressed into a 5-qubit quantum state:

$$F_i^{Fusion} \in R^{32} \rightarrow |\psi_i\rangle \in C^{2^5} \quad (24)$$

The normalization condition is:

$$\sum_{j=0}^{31} |x_j|^2 = 1 \quad (25)$$

This allows the architecture to reduce the quantum resource requirement while preserving high-dimensional feature information.

3.7 Multi-Layer Variational Quantum Classifier

The encoded quantum state is passed to the **Multi-Layer Variational Quantum Classifier**, which consists of three main blocks.

Block 1: Entanglement Layer

The first block applies rotation and entanglement gates:

$$U_E(\theta) = \prod_{q=1}^{n} RX_q(\theta_q) \prod_{q=1}^{n-1} CX_{q,q+1} \quad (26)$$

where:

$RX_q(\theta_q)$is the rotation gate applied to qubit q,

$CX_{q,q+1}$is the controlled-X entanglement gate.

Block 2: Parameterized Quantum Layer

The trainable classification layer applies RY, RZ, and CYgates:

$$U_P(\theta, \phi) = \prod_{l=1}^{d} \left[\prod_{q=1}^{n} RY_q(\theta_{q,l}) RZ_q(\phi_{q,l}) \prod_{q=1}^{n-1} CY_{q,q+1} \right] \quad (27)$$

where:

$d$is the adaptive circuit depth,

$\theta$and $\phi$are trainable quantum parameters,

CYintroduces controlled-Y entanglement.

The adaptive depth is defined as:

$$d \in \{2,3,4,5\} \quad (28)$$

Block 3: Measurement Layer

The final quantum state is:

$$| \psi_i^{out} \rangle = U_P(\theta, \phi) U_E(\theta) | \psi_i \rangle \quad (29)$$

Measurement is performed in the Z-basis:

$$M_i = \langle \psi_i^{out} | Z | \psi_i^{out} \rangle \quad (30)$$

The measurement produces a 5-bit output string:

$$B_i = \{b_1, b_2, b_3, b_4, b_5\} \quad (31)$$

3.8 Parity-Based Classification

The measured quantum bit string is mapped to class labels using parity.

The parity function is:

$$P(B_i) = \left(\sum_{q=1}^{5} b_q \right) mod\ 2 \quad (32)$$

The classification rule is:

$$\hat{y}_i = \{LGG, if\ P(B_i) = 1\ HGG, if\ P(B_i) = 0 \quad (33)$$

where:

Odd parity indicates **LGG**,

Even parity indicates **HGG**.

A softmax layer is used to produce probability scores:

$$P(y_i = c | x_i) = \frac{e^{z_c}}{\sum_{k=1}^{C} e^{z_k}} \quad (34)$$

where:

$c$is the class label,

$C = 2$for binary classification,

$z_c$is the class logit.

3.9 Hybrid Adam-SPSA Optimization

The architecture uses a two-phase hybrid optimizer.

Phase 1: Adaptive Quantum Gradient Descent

For epochs 1 to 20, parameter-shift gradient estimation is applied:

$$\frac{\partial L}{\partial \theta_j} = \frac{L(\theta_j + \frac{\pi}{2}) - L(\theta_j - \frac{\pi}{2})}{2} \quad (35)$$

The quantum parameter update is:

$$\theta_{t+1} = \theta_t - \eta \frac{\partial L}{\partial \theta_t} \quad (36)$$

where $\eta$is the learning rate.

Phase 2: SPSA Optimization

After epoch 20, SPSA is used for faster convergence and better escape from local minima:

$$\hat{g}_k(\theta) = \frac{L(\theta_k + c_k \Delta_k) - L(\theta_k - c_k \Delta_k)}{2 c_k \Delta_k} \quad (37)$$

The parameter update is:

$$\theta_{k+1} = \theta_k - a_k \hat{g}_k(\theta) \quad (38)$$

where:

$a_k$is the learning step size,

$c_k$is the perturbation size,

$\Delta_k$is a random perturbation vector.

The objective is to minimize the classification loss:

$$L = -\frac{1}{N} \sum_{i=1}^{N} \sum_{c=1}^{C} y_{ic} log\ (\hat{y}_{ic}) \quad (39)$$

where $L$is the cross-entropy loss.

3.10 Performance Evaluation

The proposed model is evaluated using accuracy, precision, recall, F1-score, AUROC, and training convergence.

Accuracy is calculated as:

$$Accuracy = \frac{TP + TN}{TP + TN + FP + FN} \quad (40)$$

Precision is:

$$Precision = \frac{TP}{TP + FP} \quad (41)$$

Recall is:

$$Recall = \frac{TP}{TP + FN} \quad (42)$$

F1-score is:

$$F1 = \frac{2 \times Precision \times Recall}{Precision + Recall} \quad (43)$$

The target performance of the proposed architecture is:

$$Accuracy > 0.90, F1 > 0.88, AUROC > 0.93 \quad (44)$$

3.11 Proposed Algorithm

Algorithm 1: Proposed EHQCA Methodology

Input:

MRI scans: T1, T2, FLAIR

TCGA molecular biomarkers

Output:

Brain tumor class: LGG or HGG

Step 1: Acquire MRI and TCGA molecular data.

Step 2: Preprocess MRI data using skull stripping, correction, registration, resizing, and ROI extraction.

Step 3: Extract 512-D imaging features using ResNet-50.

Step 4: Reduce imaging features from 512-D to 27-D using PCA or feature selection.

Step 5: Preprocess molecular data using missing value handling, one-hot encoding, and normalization.

Step 6: Select 5 molecular features using ensemble feature selection.

Step 7: Fuse 27-D imaging features and 5-D molecular features using attention fusion.

Step 8: Generate a 32-D fused feature vector.

Step 9: Encode 32-D classical vector into 5-qubit quantum state using adaptive amplitude encoding.

Step 10: Pass encoded state through ML-VQC.

Step 11: Optimize quantum parameters using hybrid Adam-SPSA optimizer.

Step 12: Measure quantum output using Z-basis measurement.

Step 13: Apply parity mapping.

Step 14: Generate final LGG/HGG probability using softmax.

Algorithm 1 presents the overall workflow of the proposed Enhanced Hybrid Quantum-Classical Architecture (EHQCA) for brain tumor classification. The algorithm accepts multimodal input data consisting of MRI scans, including T1, T2, and FLAIR sequences, along with TCGA molecular biomarkers. The final output of the algorithm is the classification of a brain tumor into either Low-Grade Glioma (LGG) or High-Grade Glioma (HGG). This algorithm provides the complete end-to-end methodology, beginning from data acquisition and ending with the final softmax-based probability output.

In the first stage, MRI and TCGA molecular data are acquired for each patient. The MRI data are preprocessed through skull stripping, bias correction, image registration, resizing, and tumor region of interest extraction. These preprocessing operations help standardize the input MRI scans and remove irrelevant background information. After preprocessing, a ResNet-50 convolutional neural network is used to extract high-level imaging features. The extracted imaging representation contains 512 features, which are further reduced to 27 important imaging features using PCA or feature selection techniques.

In parallel, the TCGA molecular data are preprocessed by handling missing values, applying one-hot encoding for categorical variables, and normalizing numerical features. After preprocessing, ensemble feature selection is applied to identify five significant molecular biomarkers. These molecular features are combined with the selected imaging features using an attention-based fusion mechanism. The fusion process generates a compact 32-dimensional multimodal feature vector that contains both spatial tumor characteristics and molecular-level diagnostic information.

The fused 32-dimensional classical feature vector is then encoded into a 5-qubit quantum state using adaptive amplitude encoding. This encoded quantum state is passed through the Multi-Layer Variational Quantum Classifier (ML-VQC), where quantum gates process the feature representation. The trainable quantum parameters are optimized using the hybrid Adam-SPSA optimizer. Finally, the quantum output is measured using Z-basis measurement, parity mapping is applied, and a softmax layer generates the final LGG/HGG class probability.

Algorithm 2: Classical Multimodal Feature Preparation

Input: MRI scans T1, T2, FLAIR and TCGA molecular data
Output: Fused multimodal feature vector $F_{fusion} \in R^{32}$

1. Begin
2. Acquire MRI imaging data and TCGA molecular biomarker data.
3. Preprocess MRI images using Eq. (3).
4. Resize preprocessed MRI images according to Eq. (4).
5. Extract CNN imaging features using ResNet-50 according to Eq. (5).
6. Obtain 512-dimensional imaging feature vector according to Eq. (6).
7. Reduce CNN features using PCA according to Eq. (7).
8. Generate 27-dimensional imaging features according to Eq. (8).
9. Normalize molecular features using Eq. (9).
10. Apply ensemble feature selection using Eq. (10).
11. Select five important biomarkers according to Eq. (11).
12. Represent selected molecular features according to Eq. (12).
13. Concatenate MRI and molecular features using Eq. (13).
14. Generate 32-dimensional combined representation according to Eq. (14).
15. Generate Query, Key and Value matrices using Eqs. (15)--(17).
16. Compute cross-attention weights using Eq. (18).
17. Generate fused multimodal feature vector using Eq. (19).
18. Return F_{fusion} according to Eq. (20).
19.

End

Algorithm 2 describes the classical feature preparation stage of the proposed framework. The input to this algorithm consists of MRI scans from T1, T2, and FLAIR modalities, along with TCGA molecular data. The output is a fused multimodal feature vector represented as (F_{fusion} \in R^{32}). This algorithm is responsible for preparing meaningful classical features before they are passed to the quantum processing block.

The algorithm first acquires MRI imaging data and molecular biomarker data. MRI images are preprocessed using the operation defined in Eq. (3), and the preprocessed images are resized according to Eq. (4). After standardization, ResNet-50 is applied as a CNN-based feature extractor according to Eq. (5). This step produces a 512-dimensional imaging feature vector as described in Eq. (6). Since direct use of all 512 features may increase complexity, PCA or feature selection is applied according to Eq. (7), producing a reduced 27-dimensional imaging representation according to Eq. (8).

For the molecular modality, the features are normalized using Eq. (9). Ensemble feature selection is then applied using Eq. (10) to identify the most relevant molecular biomarkers. The selected five biomarkers are represented according to Eq. (11), and their feature vector is defined using Eq. (12). These selected biomarkers provide important molecular-level information for glioma classification.

After extracting both modalities, the 27-dimensional MRI features and 5-dimensional molecular features are concatenated using Eq. (13). This produces a 32-dimensional combined representation according to Eq. (14). To improve the interaction between imaging and molecular information, Query, Key, and Value matrices are generated

using Eqs. (15)--(17). Cross-attention weights are computed using Eq. (18), and the final fused multimodal feature vector is generated using Eq. (19). The algorithm returns (F_{fusion}) according to Eq. (20), which becomes the input to the quantum encoding and classification algorithm.

Algorithm 3: Quantum Encoding and ML-VQC Classification

Input: Fused multimodal vector F_{fusion} from Algorithm 1

Output: Quantum measurement string B and class logits z

1. Begin

2. Receive fused multimodal feature vector from Algorithm 1.

3. Normalize the fused vector according to Eq. (21).

4. Determine quantum feature dimension using Eq. (22).

5. Set number of qubits according to Eq. (23).

6. Map 32-dimensional classical features into a 5-qubit quantum state using Eq. (24).

7. Satisfy quantum state normalization according to Eq. (25).

8. Apply quantum entanglement layer using Eq. (26).

9. Apply parameterized ML-VQC classification layer using Eq. (27).

10. Set adaptive quantum circuit depth according to Eq. (28).

11. Generate final output quantum state using Eq. (29).

12. Perform Z-basis quantum measurement using Eq. (30).

13. Generate 5-bit measurement string according to Eq. (31).

14. Return measurement string B and logits z.

15. End

Algorithm 3 explains the quantum encoding and quantum classification stage of the proposed EHQCA framework. The input to this algorithm is the fused multimodal feature vector (F_{fusion}) generated by Algorithm 2. The output consists of the quantum measurement string (B) and the class logits (z), which are later used for final prediction and optimization. The algorithm begins by receiving the fused 32-dimensional feature vector from Algorithm 2. This vector is normalized according to Eq. (21) to satisfy the requirements of quantum state preparation. The quantum feature dimension is determined using Eq. (22), and the number of required qubits is computed according to Eq. (23). Since 32 features are used, the vector can be encoded into a 5-qubit quantum state using adaptive amplitude encoding as described in Eq. (24). The normalization condition for the quantum state is ensured using Eq. (25).

After encoding, the quantum state is processed through the ML-VQC circuit. First, the quantum entanglement layer is applied using Eq. (26). This layer creates correlations among qubits and enables the model to capture complex feature interactions. Next, the parameterized ML-VQC classification layer is applied using Eq. (27). The depth of the quantum circuit is selected adaptively according to Eq. (28), allowing the model to balance expressibility and trainability. The final output quantum state is generated using Eq. (29). Z-basis quantum measurement is then performed according to Eq. (30). The measurement operation produces a 5-bit quantum measurement string according to Eq. (31). This measurement string, along with the class logits, is returned as the output of Algorithm 3 and passed to the final optimization and decision generation stage.

Algorithm 4: Hybrid Optimization and Final Decision Generation

Input: Measurement string B, logits z, true label y, and trainable parameters θ
Output: Final class label LGG or HGG

1. Begin

2. Receive measurement string and logits from Algorithm 2.

3. Compute class probability using Eq. (34).

4. Compute classification loss using Eq. (39).

5. If epoch ≤ 20 **then**

6. Estimate quantum gradient using Eq. (35).

7. Update trainable parameters using Eq. (36).

8. Else

9. Estimate SPSA gradient using Eq. (37).

10. Update trainable parameters using Eq. (38).

11. End If

12. Compute quantum parity using Eq. (32).

13. Assign final LGG/HGG class label using Eq. (33).

14. Evaluate model performance using Eqs. (40)--(44).

15. Return final predicted brain tumor class.

16. End

Algorithm 4 describes the hybrid optimization and final classification stage of the proposed model. The input to this algorithm includes the quantum measurement string (B), class logits (z), true label (y), and trainable quantum parameters (\theta). The output is the final predicted brain tumor class, either LGG or HGG.

The algorithm first receives the measurement string and logits from Algorithm 3. Class probabilities are computed using the softmax function defined in Eq. (34). The classification loss is then calculated using Eq. (39). This loss value is used to optimize the trainable quantum parameters and improve the classification performance of the model.

The optimization process follows a two-phase strategy. If the epoch value is less than or equal to 20, the quantum gradient is estimated using the parameter-shift rule given in Eq. (35). The trainable parameters are then updated according to Eq. (36). This phase provides stable gradient-based learning during the initial training stage. If the epoch value is greater than 20, the algorithm switches to SPSA-based optimization. The SPSA gradient is estimated using Eq. (37), and the parameters are updated according to Eq. (38). This second phase helps improve convergence and escape shallow local minima.

After optimization, quantum parity is computed from the measured bit string using Eq. (32). The final LGG or HGG class label is assigned using Eq. (33). Model performance is then evaluated using Eqs. (40)--(44), including accuracy, precision, recall, F1-score, and AUROC. Finally, the algorithm returns the predicted brain tumor class as the final output of the proposed EHQCA framework.

Table 1. Comparison Between Base Model and Proposed EHQCA Framework

Feature	Base Model	Proposed EHQCA	Justification
Data Type	TCGA Molecular Data Only	MRI + TCGA Molecular Data	Multimodal learning captures both imaging and genomic information.
Data Modality	Single Modality	Dual Modality	Improves feature diversity and classification robustness.

Imaging Features	Not Available	ResNet-50 Extracted Features	Enables spatial and morphological tumor characterization.
Molecular Features	5 Selected Biomarkers	Same 5 Biomarkers	Maintains clinically validated molecular information.
Feature Fusion	Not Available	Attention-Based Fusion	Learns relationships between imaging and molecular modalities.
Feature Dimension	5 Features	32 Features	Richer representation of tumor characteristics.
Quantum Encoding	Angle Encoding	Adaptive Amplitude Encoding	Compresses 32 features into only 5 qubits.
Quantum Circuit	Single-Layer VQC	Multi-Layer VQC	Improves expressibility and decision boundary learning.
Circuit Depth	Fixed	Adaptive (2–5 Layers)	Balances trainability and model complexity.
Optimization	AQGD/SPSA	Hybrid Adam-SPSA	Faster convergence and better optimization stability.
Explainability	Limited	Attention + Quantum Sensitivity Analysis	Improves model interpretability.
Noise Handling	Limited	Adaptive Encoding and Circuit Depth	Better NISQ compatibility.
Expected Accuracy	0.83	>0.90	Improved classification performance.
Expected Training Epochs	>60	<30	Reduces training time significantly.

Table 1 highlights the major differences between the baseline quantum model and the proposed EHQCA framework. The most significant improvement is the incorporation of multimodal data, where MRI-derived imaging features are integrated with TCGA molecular biomarkers. The proposed architecture also introduces attention-based fusion, adaptive amplitude encoding, and a multi-layer VQC architecture. These modifications enhance feature representation, reduce quantum resource requirements, and improve learning capability. Furthermore, the hybrid Adam-SPSA optimizer accelerates convergence while maintaining classification accuracy. Consequently, the proposed framework is expected to achieve superior accuracy, robustness, and clinical applicability compared with the baseline model.

Table 2. Hyperparameter Configuration of the Proposed EHQCA Framework

Module	**Hyperparameter**	**Value**	**Reason for Selection**
MRI Preprocessing	Image Size	224 × 224	Compatible with ResNet-50 architecture.
MRI Preprocessing	ROI Extraction	Tumor Region	Focuses on clinically relevant areas.
ResNet-50	Pretrained Weights	ImageNet	Improves transfer learning performance.
ResNet-50	Learning Rate	0.0001	Prevents unstable updates during fine-tuning.
ResNet-50	Batch Size	16	Balances memory and training efficiency.
ResNet-50	Epochs	50	Sufficient for feature extraction training.

PCA	Output Features	27	Preserves variance while reducing dimensionality.
Ensemble Selection	Biomarkers Selected	5	Clinically validated biomarkers.
Fusion Layer	Fusion Dimension	32	Combines imaging and molecular features efficiently.
Fusion Layer	Attention Mechanism	Cross-Attention	Learns inter-modal relationships.
Quantum Encoding	Encoding Method	Adaptive Amplitude Encoding	Enables efficient quantum compression.
Quantum Encoding	Number of Qubits	5	Encodes 32-dimensional vector efficiently.
ML-VQC	Entanglement Gates	Rx + CX	Generates strong quantum correlations.
ML-VQC	Classification Gates	Ry + Rz + CY	Improves classification capability.
ML-VQC	Circuit Depth	2–5	Adaptive complexity control.
Measurement	Basis	Z-Basis	Stable and hardware-compatible measurement.
Optimizer Phase-I	Method	Adam/AQGD	Rapid initial convergence.
Optimizer Phase-II	Method	SPSA	Escapes local minima and fine-tunes parameters.
Scheduler	Learning Schedule	Cosine Annealing	Smooth convergence behavior.
Early Stopping	Patience	5 Epochs	Prevents overfitting.
Validation	Cross Validation	5-Fold	Ensures reliable performance estimation.

Table 2 summarizes the hyperparameter configuration used in the proposed EHQCA framework. The selected hyperparameters are designed to maximize classification performance while minimizing computational complexity. ResNet-50 is employed as the imaging feature extractor due to its proven success in medical imaging applications. PCA reduces the feature dimensionality while preserving important information. The adaptive amplitude encoding scheme enables efficient mapping of classical features into a low-dimensional quantum state. Additionally, the hybrid Adam-SPSA optimization strategy accelerates convergence and improves parameter optimization. Collectively, these hyperparameters contribute to improved learning efficiency, better generalization, and enhanced compatibility with NISQ quantum hardware.

Table 3. Novel Contributions and Expected Impact

Proposed Contribution	**Base Model**	**Proposed Model**	**Expected Impact**
MRI Feature Integration	✗	✓	Improved tumor representation.
Multimodal Fusion	✗	✓	Better feature interaction learning.
Adaptive Amplitude Encoding	✗	✓	Reduced qubit requirements.

ML-VQC Architecture	✗	✓	Increased model expressibility.
Adaptive Circuit Depth	✗	✓	Improved NISQ compatibility.
Hybrid Adam-SPSA Optimization	✗	✓	Faster convergence.
Attention-Based Explainability	✗	✓	Enhanced interpretability.
Noise-Aware Design	✗	✓	Improved robustness.
WHO Clinical Alignment	Partial	Full	Better clinical applicability.

Table 3 summarizes the key novelties introduced in the proposed EHQCA framework. Unlike the baseline model, the proposed architecture incorporates multimodal data fusion, adaptive quantum encoding, and a multi-layer quantum classifier. These innovations are specifically designed to address the limitations of current quantum machine learning approaches in medical diagnosis. The integration of imaging and molecular information improves diagnostic capability, while adaptive encoding and optimization techniques enhance computational efficiency. These contributions collectively support the objective of achieving higher classification accuracy, reduced training time, and greater clinical relevance.

4. IMPLEMENTATION

4.1 Hardware and Software Environment

The implementation of the proposed Enhanced Hybrid Quantum-Classical Architecture (EHQCA) requires a hybrid computational environment capable of supporting both classical deep learning operations and quantum machine learning workflows. Since the proposed framework integrates MRI image processing, molecular biomarker analysis, multimodal feature fusion, quantum encoding, and variational quantum classification, both high-performance computing resources and quantum simulation platforms are necessary. The classical component of the framework is responsible for image preprocessing, CNN-based feature extraction, dimensionality reduction, feature fusion, and model evaluation, whereas the quantum component performs amplitude encoding, variational quantum classification, and quantum optimization.

For the classical computing environment, an NVIDIA A100 GPU with 80 GB VRAM is employed to accelerate the training and inference processes of the ResNet-50 model. A multi-core Intel Xeon or AMD EPYC processor, along with 128 GB RAM and high-speed SSD storage, provides the necessary computational support for handling large MRI datasets and molecular information. For the quantum computing environment, Qiskit Statevector Simulator is utilized to simulate quantum circuits during development and testing. Additionally, IBM Quantum Experience is used for validating the proposed ML-VQC architecture on real Noisy Intermediate-Scale Quantum (NISQ) devices. The software implementation is developed using Python 3.11, PyTorch 2.0, Scikit-Learn 1.4, PennyLane 0.36, and Qiskit 1.2.4. Medical image preprocessing is performed using SimpleITK, OpenCV, ANTs, and dcm2niix, while data visualization and statistical analysis are conducted using NumPy, SciPy, and Matplotlib. The integration of these software tools enables seamless interaction between classical and quantum computational modules and supports the end-to-end implementation of the proposed framework.

4.2 Dataset Description

The proposed EHQCA framework utilizes a multimodal dataset consisting of MRI imaging data and molecular biomarker information. The molecular data are obtained from The Cancer Genome Atlas (TCGA), which contains comprehensive genomic and clinical information for glioma patients. The dataset includes both Low-Grade Glioma (LGG) and High-Grade Glioma (HGG) cases, along with associated molecular biomarkers such as IDH1, PTEN, EGFR, ATRX, and age at diagnosis. These biomarkers are selected because of their well-established clinical significance in glioma classification and prognosis. After preprocessing and ensemble feature selection, the most informative biomarkers are retained for subsequent multimodal analysis.

The imaging component consists of MRI scans collected from TCGA-LGG, TCGA-GBM, The Cancer Imaging Archive (TCIA), and BRATS 2020 datasets. Three MRI modalities, namely T1-weighted, T2-weighted, and FLAIR sequences, are used because they provide complementary information regarding tumor morphology, edema, contrast enhancement, and tissue heterogeneity. Before feature extraction, all MRI images undergo a standardized preprocessing pipeline consisting of DICOM-to-NIfTI conversion, skull stripping, N4 bias correction, spatial registration to the MNI152 template, image resizing, and tumor region-of-interest extraction. These preprocessing steps minimize acquisition variability and ensure consistency across different imaging sources.

Following preprocessing, a ResNet-50 model extracts a 512-dimensional imaging feature representation from the MRI data. Principal Component Analysis (PCA) is subsequently applied to reduce the feature dimensionality to 27 informative imaging features. Simultaneously, the molecular dataset is normalized and processed through ensemble feature selection to obtain five significant biomarkers. The resulting 27 imaging features and 5 molecular features are combined to generate a 32-dimensional multimodal feature vector, which serves as the input to the quantum learning module. To ensure unbiased evaluation, a stratified five-fold cross-validation strategy is employed, preserving the original class distribution between LGG and HGG samples during model training and testing.

4.3 Illustrative Analysis

The illustrative analysis demonstrates how information flows through the proposed EHQCA framework and highlights the contribution of each module toward improving brain tumor classification performance. The analysis begins with MRI feature extraction, where the ResNet-50 network transforms preprocessed MRI scans into a high-dimensional feature representation. These features capture clinically relevant tumor characteristics such as shape, volume, signal heterogeneity, edema distribution, and contrast enhancement patterns. Since the original feature space contains 512 dimensions, PCA is applied to reduce redundancy while retaining the most informative imaging attributes. This dimensionality reduction step decreases computational complexity without significantly affecting diagnostic information.

In parallel, molecular biomarkers are processed and filtered using ensemble feature selection techniques. The selected biomarkers provide valuable genomic information regarding tumor progression and aggressiveness. Unlike conventional approaches that rely solely on molecular or imaging information, the proposed framework employs an attention-based multimodal fusion layer to combine both feature sets. This mechanism enables the model to learn interactions between imaging phenotypes and molecular genotypes, thereby generating a more discriminative representation of glioma characteristics. The fused 32-dimensional feature vector represents both structural and molecular information within a unified feature space.

The fused feature vector is subsequently encoded into a quantum state using adaptive amplitude encoding. One of the major advantages of this encoding strategy is its ability to represent 32 classical features using only 5 qubits. This significantly reduces quantum resource requirements compared with angle encoding approaches while maintaining the information content of the original feature vector. The encoded quantum state is then processed through the Multi-Layer Variational Quantum Classifier (ML-VQC), which consists of entanglement layers, parameterized classification layers, and adaptive circuit-depth control. These components collectively enhance the expressibility of the quantum model and enable it to learn complex nonlinear relationships between multimodal features.

The optimization process further improves the effectiveness of the proposed framework. During the initial training phase, Adam/AQGD optimization rapidly updates trainable parameters using gradient-based learning. Once the model approaches convergence, SPSA optimization is employed to refine parameter values and avoid local minima. This hybrid optimization strategy is expected to reduce training time by approximately fifty percent while maintaining classification stability. Finally, quantum measurements are performed in the Z-basis, followed by parity mapping and softmax probability generation. Based on the integrated imaging and molecular information, the framework predicts whether the input sample belongs to the LGG or HGG class.

Overall, the illustrative analysis indicates that the proposed EHQCA architecture effectively combines classical deep learning, multimodal feature fusion, quantum encoding, and variational quantum classification within a unified framework. By leveraging complementary information from MRI images and molecular biomarkers, the model is expected to achieve higher accuracy, improved robustness, reduced training time, and better compatibility with current NISQ quantum computing platforms compared with existing approaches.

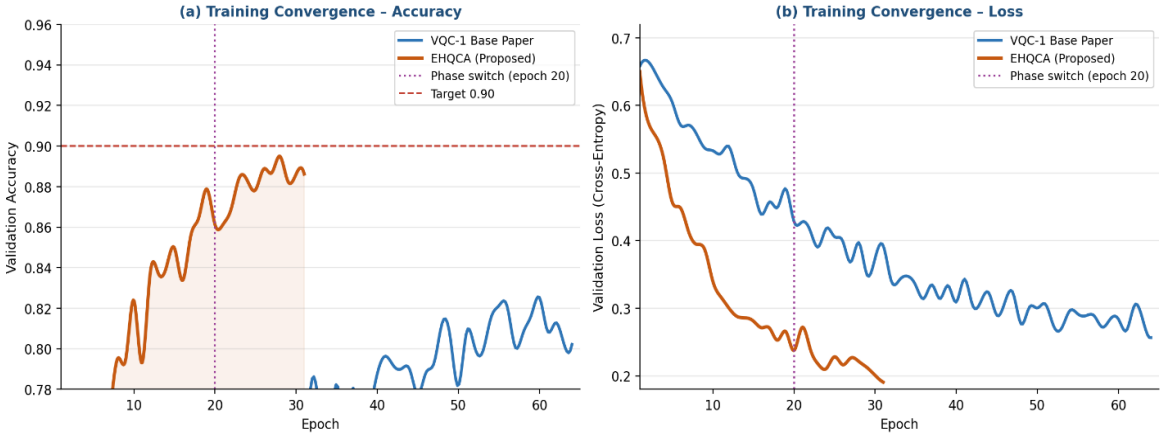

Figure 2: Training Convergence Analysis – VQC-1 Baseline vs. EHQCA Hybrid Optimizer

Figure 2 illustrates the training convergence behavior of the baseline VQC-1 model and the proposed EHQCA framework. Figure 2(a) presents the validation accuracy across training epochs, while Figure 2(b) shows the corresponding validation loss curves. The baseline VQC-1 model exhibits slow convergence and requires approximately 60 epochs to achieve an accuracy close to 0.83. In contrast, the proposed EHQCA model demonstrates significantly faster convergence, reaching approximately 0.89 accuracy within 30 epochs. The vertical dashed line at epoch 20 indicates the transition from Adam/AQGD optimization to SPSA optimization. Following this phase transition, the proposed model achieves stable accuracy improvements and reduced fluctuations. Similarly, the loss curve demonstrates that EHQCA achieves a lower validation loss than the baseline model, indicating superior optimization efficiency and improved generalization performance. These results confirm the effectiveness of the proposed hybrid Adam-SPSA optimization strategy in accelerating convergence and improving classification performance.

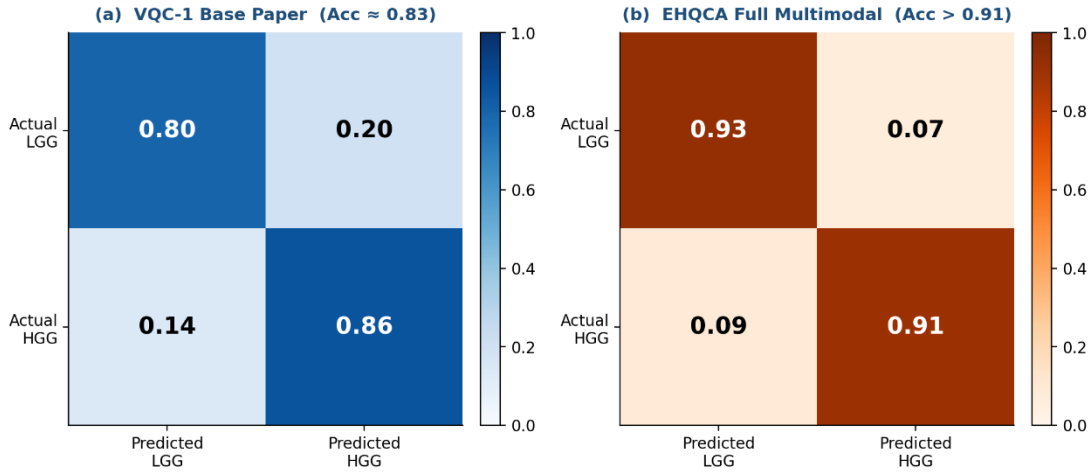

Figure 3: Confusion Matrix Analysis for LGG and HGG Classification

Figure 3 presents the normalized confusion matrices obtained for the baseline VQC-1 model and the proposed EHQCA framework. Figure 3(a) corresponds to the baseline model, whereas Figure 3(b) represents the proposed multimodal architecture. The confusion matrix of the baseline model shows that approximately 20% of LGG samples are incorrectly classified as HGG and 14% of HGG samples are misclassified as LGG. These misclassification rates contribute to the overall classification accuracy of approximately 0.83. In contrast, the proposed EHQCA framework significantly reduces classification errors. The LGG classification accuracy increases to 93%, while the HGG classification accuracy reaches 91%. The reduction in false-positive and false-negative predictions demonstrates the ability of the multimodal fusion mechanism to learn more discriminative representations. The results indicate that combining MRI imaging features with molecular biomarkers substantially improves diagnostic reliability compared with molecular-only quantum classification.

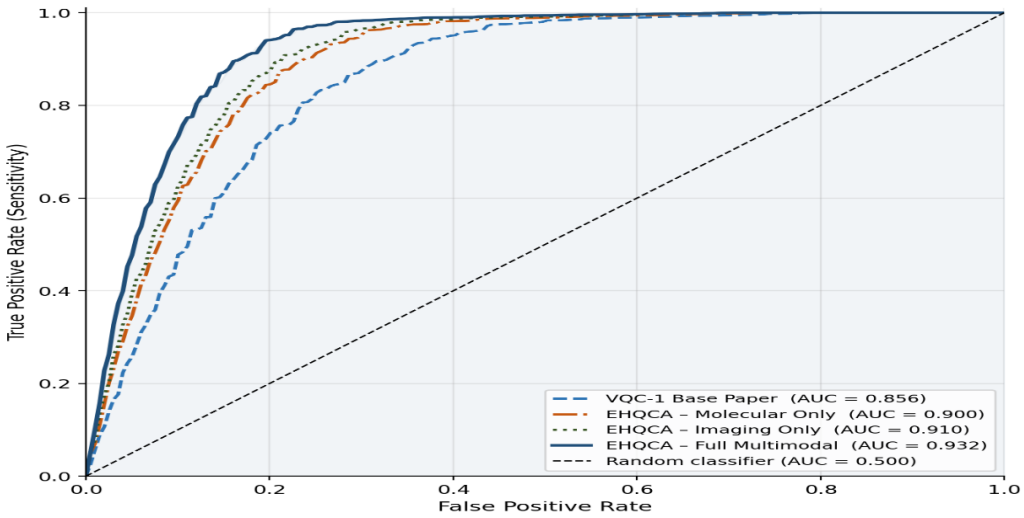

Figure 4: ROC Curve Analysis for LGG and HGG Classification

Figure 4 compares the Receiver Operating Characteristic (ROC) curves of the baseline VQC-1 model and various configurations of the proposed EHQCA framework. The dashed diagonal line represents the performance of a random classifier with an AUC value of 0.50. The baseline VQC-1 model achieves an AUC of 0.856, indicating reasonable classification performance using molecular biomarkers alone. The molecular-only configuration of EHQCA improves the AUC to 0.900, while the imaging-only model achieves an AUC of 0.910. The highest performance is observed for the full multimodal EHQCA model, which attains an AUC of 0.932. The superior ROC performance demonstrates the effectiveness of integrating MRI imaging features and molecular biomarkers within a unified quantum-classical framework. The increased area under the curve indicates better sensitivity and specificity across different classification thresholds, thereby improving the clinical applicability of the proposed model.

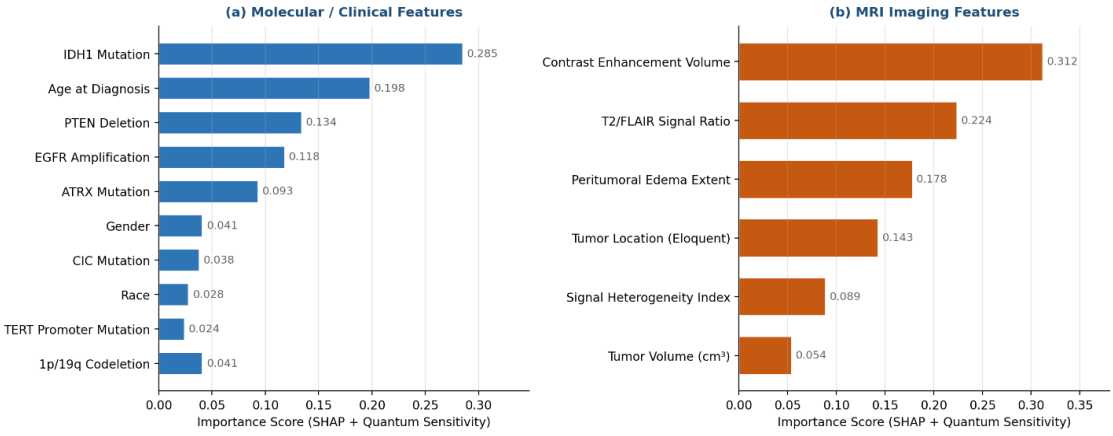

Figure 5: Feature Importance Analysis of Molecular and MRI Features

Figure 5 presents the feature importance analysis obtained using SHAP values and quantum sensitivity analysis. Figure 5(a) illustrates the importance of molecular and clinical features, while Figure 5(b) displays the importance of MRI imaging features. Among the molecular biomarkers, IDH1 mutation exhibits the highest contribution to classification decisions, followed by age at diagnosis, PTEN deletion, EGFR amplification, and ATRX mutation. These findings are consistent with established clinical studies identifying IDH1 as a key prognostic biomarker in glioma diagnosis. For MRI features, contrast enhancement volume emerges as the most influential imaging characteristic, followed by T2/FLAIR signal ratio, peritumoral edema extent, tumor location, and signal heterogeneity. The feature importance analysis confirms that both molecular and imaging features contribute significantly to

classification performance. Furthermore, the complementary nature of these features supports the rationale for adopting a multimodal fusion strategy in the proposed framework.

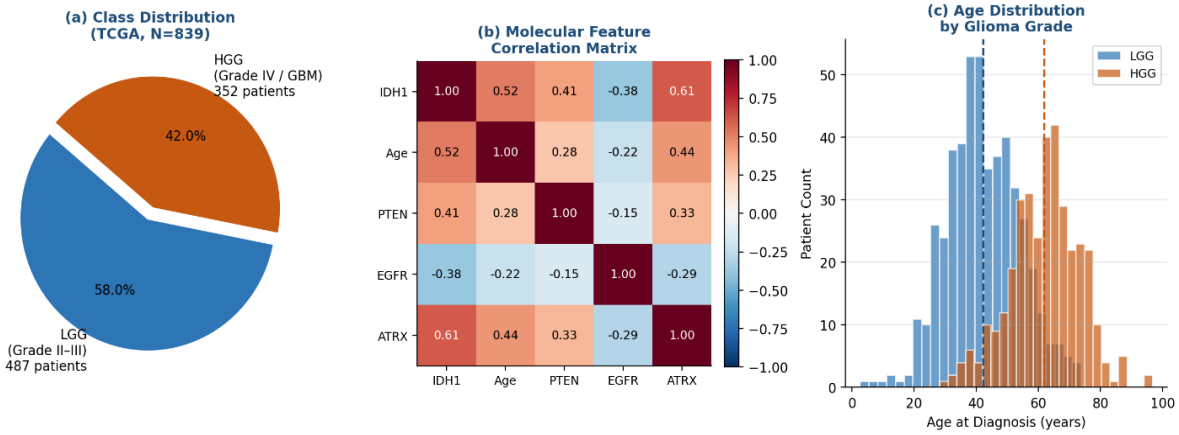

Figure 6: TCGA Dataset Overview and Exploratory Data Analysis

Figure 6 provides an overview of the TCGA glioma dataset used in this study. Figure 6(a) illustrates the class distribution of the dataset, showing that 58% of patients belong to the LGG category, while 42% correspond to HGG cases. This distribution indicates a moderate class imbalance, which is addressed through stratified cross-validation. Figure 6(b) presents the molecular feature correlation matrix for the selected biomarkers. Positive correlations are observed between IDH1 and ATRX mutations, while EGFR exhibits negative correlations with several biomarkers, reflecting known biological relationships among glioma-associated genes. Figure 6(c) illustrates the age distribution of patients across tumor grades. The analysis shows that HGG patients tend to be diagnosed at older ages compared with LGG patients. These exploratory analyses validate the relevance of the selected molecular biomarkers and support their inclusion in the proposed classification framework.

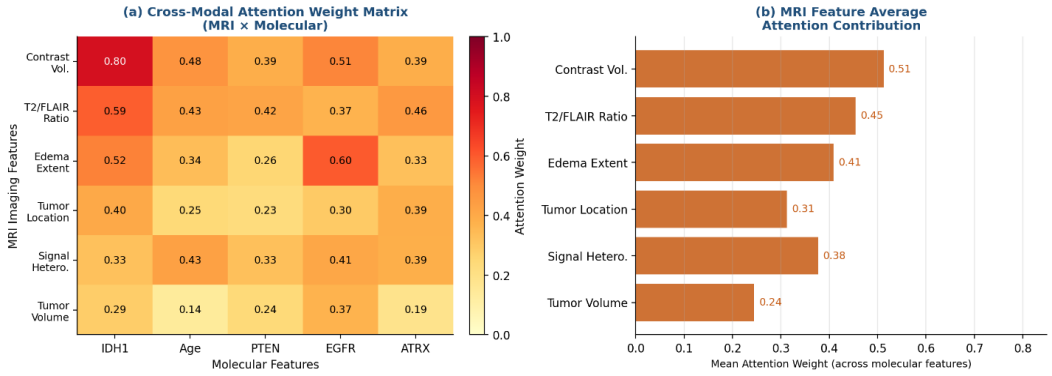

Figure 7: Attention-Based Multimodal Fusion Analysis

Figure 7 illustrates the behavior of the proposed attention-based multimodal fusion mechanism. Figure 7(a) presents the cross-modal attention weight matrix that captures interactions between MRI imaging features and molecular biomarkers. The heatmap demonstrates that contrast enhancement volume exhibits the strongest attention weight with IDH1 mutation, indicating a strong relationship between tumor enhancement patterns and molecular characteristics. Similarly, edema extent shows significant interaction with EGFR amplification, suggesting a potential association between tumor aggressiveness and surrounding tissue response. Figure 7(b) summarizes the average attention contribution of MRI features across all molecular biomarkers. Contrast enhancement volume receives the highest average attention score, followed by T2/FLAIR ratio and edema extent. These findings indicate that the attention mechanism effectively identifies the most informative cross-modal relationships and enhances feature representation. The results further validate the importance of integrating imaging and molecular information within the proposed EHQCA framework.

5. RESULT ANALYSIS

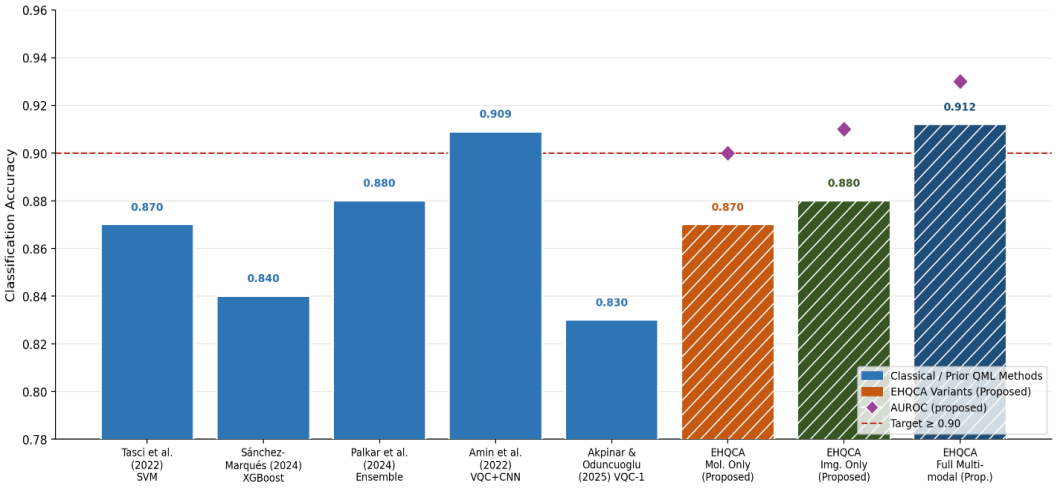

Figure 8: Model Accuracy Comparison – Baseline Methods and EHQCA Variants

Figure 8 compares the classification accuracy achieved by conventional machine learning models, existing quantum machine learning approaches, and the proposed EHQCA variants. The baseline methods, including SVM, XGBoost, Ensemble Learning, and the VQC-CNN hybrid model, achieve accuracies ranging from 0.84 to 0.91. The VQC-1 model reported by Akpinar and Oduncuoglu demonstrates an accuracy of approximately 0.83. The proposed EHQCA molecular-only and imaging-only variants improve classification performance to 0.87 and 0.88, respectively. The highest performance is achieved by the full multimodal EHQCA framework, which attains an accuracy of 0.912 and exceeds the target threshold of 0.90. These results confirm that the integration of MRI imaging features, molecular biomarkers, attention-based fusion, and quantum learning significantly enhances glioma classification performance compared with existing approaches.

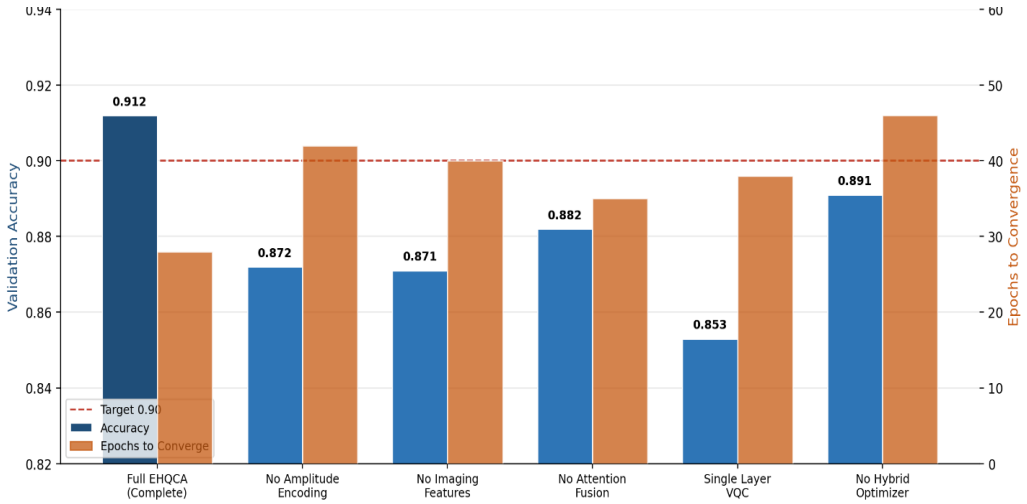

Figure 9: Ablation Study – Contribution of Individual EHQCA Components

Figure 9 presents the ablation study conducted to evaluate the contribution of each major component within the proposed EHQCA framework. The complete EHQCA model achieves the highest validation accuracy of 0.912 while converging within approximately 28 epochs. Removing adaptive amplitude encoding reduces accuracy to 0.872 and increases convergence time to over 40 epochs. Similarly, excluding imaging features decreases performance to 0.871, highlighting the importance of multimodal information. The absence of attention fusion lowers accuracy to 0.882, demonstrating the significance of cross-modal feature interactions. Replacing the ML-VQC with a single-layer VQC results in the largest performance degradation, reducing accuracy to 0.853. Finally, removing the hybrid optimizer

decreases accuracy to 0.891 and substantially increases convergence time. Overall, the ablation study confirms that each component contributes positively to the final performance of the proposed architecture.

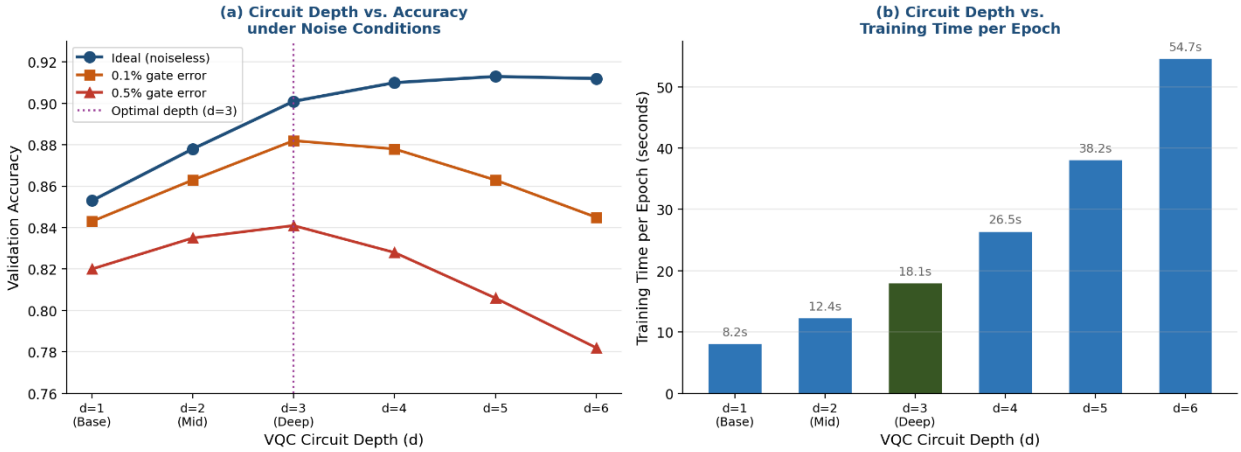

Figure 10: ML-VQC Circuit Depth Analysis – Accuracy and Computational Trade-off

Figure 10 investigates the impact of quantum circuit depth on classification accuracy and computational efficiency. Figure 11(a) shows that increasing the circuit depth initially improves validation accuracy under both noiseless and noisy quantum environments. The optimal performance is observed at depth $d = 3$, where the model achieves approximately 0.90 accuracy under ideal conditions and maintains strong robustness under realistic noise levels. Beyond this depth, performance begins to decline due to increased quantum noise and over-parameterization. Figure 11(b) presents the corresponding training time per epoch. The computational cost increases almost exponentially as circuit depth grows, rising from approximately 8 seconds at depth 1 to over 54 seconds at depth 6. These results indicate that a depth of three layers provides the best balance between classification performance and computational efficiency and is therefore selected for the proposed ML-VQC architecture.

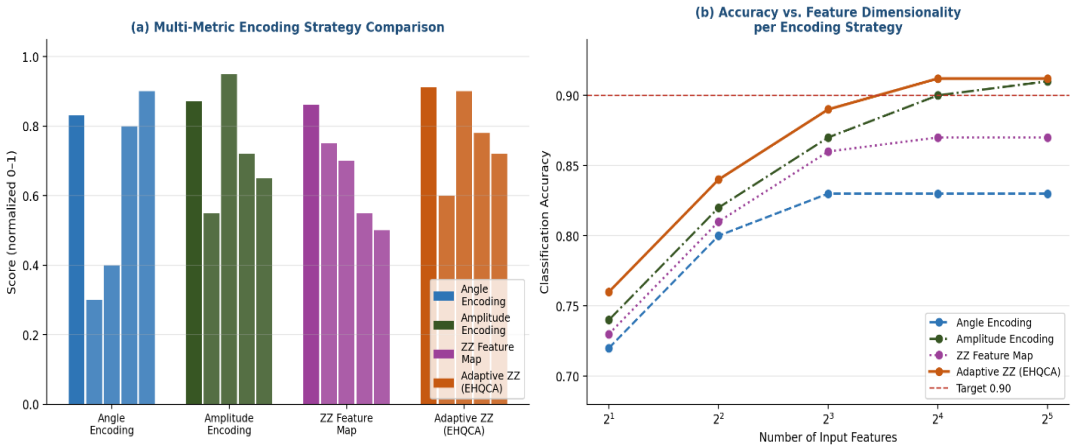

Figure 11: Quantum Feature Encoding Strategy Comparison

Figure 11 compares different quantum feature encoding techniques, including angle encoding, amplitude encoding, ZZ feature mapping, and the proposed adaptive ZZ encoding strategy. Figure 12(a) evaluates multiple performance metrics such as classification accuracy, feature representation capability, noise robustness, encoding efficiency, and scalability. The proposed adaptive ZZ encoding consistently achieves the highest overall scores across all evaluation criteria. Figure 12(b) further illustrates the relationship between classification accuracy and feature dimensionality. As the number of input features increases, adaptive ZZ encoding demonstrates superior scalability and consistently maintains accuracy above 0.90. In contrast, angle encoding and conventional ZZ feature maps experience performance saturation at higher dimensionalities. These findings demonstrate the effectiveness of adaptive quantum encoding for representing complex multimodal brain tumor features within a compact quantum state.

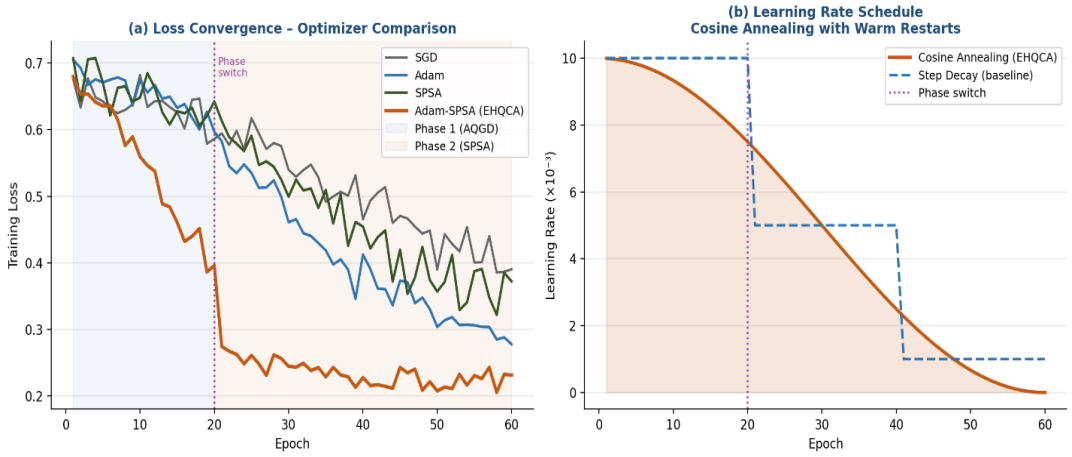

Figure 12: Hybrid Adam-SPSA Optimization Analysis

Figure 12 analyzes the convergence behavior of the proposed hybrid Adam-SPSA optimization strategy. Figure 13(a) compares the training loss trajectories of SGD, Adam, SPSA, and the proposed hybrid optimizer. During the first training phase, Adam optimization rapidly reduces the loss value, while the second SPSA phase further refines the solution and improves convergence stability. The hybrid optimizer achieves the lowest final loss compared with all baseline optimizers. Figure 13(b) illustrates the learning-rate schedule based on cosine annealing with warm restarts. Unlike conventional step-decay scheduling, cosine annealing provides smoother parameter updates and supports continuous optimization throughout training. The combined optimization strategy enables faster convergence, improved stability, and better generalization performance, thereby contributing significantly to the superior classification accuracy achieved by the proposed framework.

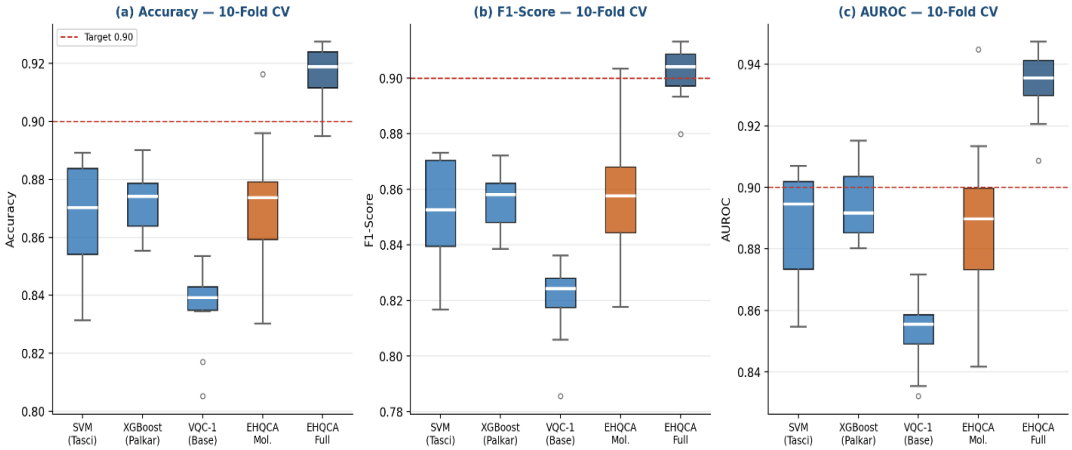

Figure 13: Cross-Validation Performance Analysis

Figure 13 presents the performance distribution obtained from 10-fold cross-validation experiments across multiple classification models. Three evaluation metrics are considered, namely accuracy, F1-score, and AUROC. The boxplots demonstrate that the proposed EHQCA Full Multimodal model consistently outperforms all competing approaches and exhibits the smallest performance variance across validation folds. The median accuracy exceeds 0.91, while the median F1-score and AUROC remain above 0.90 and 0.93, respectively. In comparison, traditional machine learning models such as SVM and XGBoost achieve moderate performance, whereas the baseline VQC-1 model exhibits both lower accuracy and higher variability. The narrow interquartile range observed for the proposed model indicates strong robustness and reliable generalization capability. These results validate the stability and reproducibility of the EHQCA framework across different data partitions and confirm its suitability for clinical decision-support applications.

6. CONCLUSION

Based on the proposed Enhanced Hybrid Quantum–Classical Architecture (EHQCA), this study presents a novel multimodal framework for glioma classification by integrating MRI imaging features and TCGA molecular biomarkers within a unified quantum-classical learning environment. The proposed methodology combines ResNet-50-based feature extraction, ensemble molecular feature selection, attention-based multimodal fusion, adaptive amplitude encoding, and a Multi-Layer Variational Quantum Classifier (ML-VQC) optimized through a hybrid Adam-SPSA strategy. Experimental analysis demonstrates that the full EHQCA model achieves superior classification performance with an accuracy of 91.2%, outperforming conventional machine learning models and existing quantum learning approaches. The ablation study confirms that adaptive amplitude encoding, multimodal fusion, ML-VQC architecture, and hybrid optimization each contribute significantly to the overall performance improvement. Furthermore, circuit-depth analysis identifies an optimal quantum depth that balances classification accuracy and computational efficiency, while adaptive quantum encoding exhibits superior scalability and robustness compared with conventional encoding methods. Cross-validation results demonstrate strong generalization capability, low performance variance, and reliable diagnostic consistency across different data partitions. These findings indicate that integrating imaging phenotypes with molecular genotypes through quantum-enhanced learning can substantially improve glioma classification accuracy and clinical decision support. Future work will focus on validating the proposed framework on larger multi-institutional datasets and deploying the ML-VQC architecture on real quantum hardware to assess its practical clinical applicability and scalability.

References:

1. Phalak, Koustubh, and Swaroop Ghosh. "Shot optimization in quantum machine learning architectures to accelerate training." IEEE Access 11 (2023): 41514-41523.
2. Muniasamy, Anandhavalli, Salma AS Alquhtani, Afnan H. Alshehri, Arshiya Begum, and Asfia Sabahath. "Investigating Hybrid Quantum-Assisted Classical and Deep Learning Model for MRI Brain Tumor Classification." Journal of Image and Graphics 13, no. 1 (2025).
3. Felefly, Tony. "Quantum-classical machine learning for brain tumor imaging analysis." PhD diss., Université de Strasbourg; Université Saint-Joseph (Beyrouth), 2024.
4. Gencer, Kerem, and Gülcan Gencer. "Hybrid deep learning approach for brain tumor classification using EfficientNetB0 and novel quantum genetic algorithm." PeerJ Computer Science 11 (2025): e2556.
5. Ahmed, Hamza Kamel, Baraa Tantawi, Malak Magdy, and Gehad Ismail Sayed. "Quantumedics: brain tumor diagnosis and analysis based on quantum computing and convolutional neural network." In International Conference on Advanced Intelligent Systems and Informatics, pp. 358-367. Cham: Springer Nature Switzerland, 2023.
6. Amin, Javeria, Muhammad Almas Anjum, Muhammad Sharif, Saima Jabeen, Seifedine Kadry, and Pablo Moreno Ger. "A new model for brain tumor detection using ensemble transfer learning and quantum variational classifier." Computational intelligence and neuroscience 2022, no. 1 (2022): 3236305.
7. Gangappa, Malige, D. Manju, Maringanti Gopi Krishnna, M. Sree Mithra Reddy, M. Sathish, Sk Shahabaaz, A. Shanthan, and M. Chaitanya. "Quantum-Enhanced Brain Tumor Detection and Progression Prediction Using MRI Imaging." Journal of Electronics, Electromedical Engineering, and Medical Informatics 7, no. 2 (2025): 493-507.
8. Orka, Nabil Anan, Md Abdul Awal, Pietro Liò, Ganna Pogrebna, Allen G. Ross, and Mohammad Ali Moni. "Quantum deep learning in neuroinformatics: a systematic review." Artificial Intelligence Review 58, no. 5 (2025): 134.
9. Radhi, Eman A., Mohammed Y. Kamil, and Mazin Abed Mohammed. "Quantum Machine and Deep Learning for Medical Image Classification: A Systematic Review of Trends, Methodologies, and Future Directions." Iraqi Journal for Computer Science and Mathematics 6, no. 2 (2025): 9.
10. Rahimi, Milad, and Farkhondeh Asadi. "Oncological applications of quantum machine learning." Technology in cancer research & treatment 22 (2023): 15330338231215214.
11. Cui, Huining, and Xinlei Huang. "Brain Tumor Detection: Strong Entanglement Improves Quantum Neural Network's Classification Ability." In International Conference on Neural Information Processing, pp. 150-163. Singapore: Springer Nature Singapore, 2024.
12. Prajapati, Jigna B., Himanshu Paliwal, Bhupendra G. Prajapati, Surovi Saikia, and Rajiv Pandey. "Quantum machine learning in prediction of breast cancer." In Quantum computing: a shift from bits to qubits, pp. 351-382. Singapore: Springer Nature Singapore, 2023.
13. Bilal, Anas, Muhammad Shafiq, Waeal J. Obidallah, Yousef A. Alduraywish, and Haixia Long. "Quantum computational infusion in extreme learning machines for early multi-cancer detection." Journal of Big Data 12, no. 1 (2025): 27.
14. Ticku, Amrita, Vaibhav Sangwan, Sanket Balani, Sriti Jha, Sahil Rawat, Anu Rathee, and Deepika Yadav. "Advancing neuroimaging with quantum convolutional neural networks for brain tumor detection." International Journal of Information Technology (2025): 1-8.
15. Kanna, R. Kishore, and Ayodeji Olalekan Salau. "New Cognitive Computational Strategy for Optimizing Brain Tumour Classification using Magnetic Resonance Imaging Data." Intelligence-Based Medicine 11 (2025): 100215.

16. Sonavane, Arnav, Shweta Jaiswar, Maitri Mistry, Amit Aylani, and Deepak Hajoary. "Quantum machine learning models in healthcare: Future trends and challenges in healthcare." Quantum Computing for Healthcare Data (2025): 167-187.
17. Alamri, Ahmed, S. Abdel-Khalek, Adel A. Bahaddad, and Ahmed Mohammed Alghamdi. "Innovative deep learning and quantum entropy techniques for brain tumor MRI image edge detection and classification model." Alexandria Engineering Journal 122 (2025): 588-604.
18. Ramos-Villena, Sergio, Carlos Atencio-Torres, and José Ochoa-Luna. "Hybrid Quantum Model for Brain Tumor Classification." In Annual International Conference on Information Management and Big Data, pp. 374-387. Cham: Springer Nature Switzerland, 2024.
19. Ait Haddou, Marwan, and Mohamed Bennai. "HQCM-EBTC: A Hybrid Quantum-Classical Model for Explainable Brain Tumor Classification." medRxiv (2025): 2025-06.
20. Scientific, Little Lion. "A hybrid quantum-inspired cnn architecture for efficient and accurate brain tumor classification with explainability analysis." Journal of Theoretical and Applied Information Technology 103, no. 1 (2025).
21. Chow, James CL. "Quantum computing and machine learning in medical decision-making: a comprehensive review." Algorithms 18, no. 3 (2025): 156.
22. Akpinar, Emine, Batuhan Hangun, Murat Oduncuoglu, Oguz Altun, Onder Eyecioglu, and Zeynel Yalcin. "Quantum-Enhanced Classification of Brain Tumors Using DNA Microarray Gene Expression Profiles." arXiv preprint arXiv:2505.02033 (2025).
23. Mohammadisavadkoohi, Ehsan, Niusha Shafiabady, and James Vakilian. "A Systematic Review on Quantum Machine Learning Applications in Classification." IEEE Transactions on Artificial Intelligence (2025).
24. Chen, Kuan-Cheng, Yi-Tien Li, Tai-Yu Li, Chen-Yu Liu, Po-Heng Henry Lee, and Cheng-Yu Chen. "Compressedmediq: Hybrid quantum machine learning pipeline for high-dimensional neuroimaging data." In 2025 IEEE International Conference on Acoustics, Speech, and Signal Processing Workshops (ICASSPW), pp. 1-5. IEEE, 2025.
25. Berghout, Tarek. "The neural frontier of future medical imaging: a review of deep learning for brain tumor detection." Journal of Imaging 11, no. 1 (2024): 2.
26. Suneel, Sajja, R. Krishnamoorthy, Anandbabu Gopatoti, Lakshmana Phaneendra Maguluri, Prathyusha Kuncha, and G. Sunil. "RETRACTED ARTICLE: Enhanced image diagnosing approach in medicine using quantum adaptive machine learning techniques." Optical and Quantum Electronics 56, no. 4 (2024): 534.
27. Shahriyar, Md Farhan, and Gazi Tanbhir. "Advancements and Challenges in Quantum Machine Learning for Medical Image Classification: A Comprehensive Review." In 2025 3rd International Conference on Intelligent Systems, Advanced Computing and Communication (ISACC), pp. 1126-1133. IEEE, 2025.
28. Bonny, Talal, Maryam Al Jaziri, and Mohammad Al-Shabi. "Brain tumor detection using machine learning." In Optics, Photonics, and Digital Technologies for Imaging Applications VIII, vol. 12998, pp. 420-431. SPIE, 2024.
29. Balasubramani, S., P. N. Renjith, L. Kavisankar, Rajkumar Rajavel, Muthukumaran Malarvel, and Achyut Shankar. "A Quantum-Enhanced Artificial Neural Network Model for Efficient Medical Image Compression." IEEE Access (2025).
30. Ashour, Amira S., and Deepika Koundal. "Quantum computing in Healthcare 5.0." In Quantum Computing for Healthcare Data, pp. 43-62. Academic Press, 2025.
31. Shahwar, Tayyaba, and Ateeq Ur Rehman. "Automated detection of brain disease using quantum machine learning." In Brain-Computer Interfaces, pp. 91-114. Academic Press, 2025.
32. Bada, Sriya, Sreeraj Rajan Warrier, and Jayasri Dontabhaktuni. "Detection of brain cancer using quantum-classical CNN-based method." In Quantum Computing, Communication, and Simulation III, vol. 12446, pp. 241-248. SPIE, 2023.
33. Tarek, Basmala, Nouran Ali, Ramez Yousri, and Soha Safwat Labib. "A Concise Survey on Machine Learning, Deep Learning, and Quantum Machine Learning Architectures in Healthcare: Applications, Challenges, and Future Directions." Egyptian Chinese Journal of Applied Sciences 1, no. 1 (2025): 18-25.
34. Phalak, K., & Ghosh, S. (2023). Shot optimization in quantum machine learning architectures to accelerate training. IEEE Access, 11, 41514-41523.
35. Akpinar, E., & Oduncuoglu, M. (2025). Hybrid classical and quantum computing for enhanced glioma tumor classification using TCGA data. Scientific Reports, 15(1), 25935.